AIAA JOURNAL
Vol. 44, No. 7, July 2006

# Semi-Active Vibration Control of Adaptive Structures Using Magnetorheological Dampers

Aurelio Dominguez*
*Universidad Autonoma de Queretaro, 76010 Queretaro, Mexico*
and
Ramin Sedaghati† and Ion Stiharu‡
*Concordia University, Montreal, Quebec H3G 1M8, Canada*

DOI: 10.2514/1.18402

**In this study a semi-active vibration control strategy has been proposed to suppress the vibration in discrete structures using magnetorheological dampers. The strategy is based on the absolute velocity at the end of the magnetorheological damper in local coordinates and the hysteresis force experienced by the magnetorheological damper. To obtain the hysteresis force, a new nonlinear hysteresis dynamic model is employed. The model determines the hysteresis force considering the amplitude, frequency, and current excitation as independent variables. Subsequently, based on this model, the finite element formulation of the magnetorheological damper is derived and incorporated into the finite element formulation of the space truss structure with integrated magnetorheological damper to simulate the response of the adaptive structure. The Newmark $\beta$ method with inner iterative algorithm is applied to solve the resulting nonlinear system. The experimental study has also been conducted to validate the finite element model. The efficiency of the proposed vibration suppression strategy has been tested against harmonic, transient, and random excitations. It has been demonstrated that the vibration can be efficiently suppressed by the controllable magnetorheological dampers.**

## Nomenclature

| | | |
|---|---|---|
| $\boldsymbol{C}$ | = | global damping matrix of the whole system |
| $c_0$ | = | damping of the MR damper |
| $I$ | = | current excitation |
| $I_c$ | = | critical current excitation |
| $I_{\max}, I_{\min}$ | = | maximum and minimum applied current excitation |
| $\boldsymbol{K}$ | = | global stiffness matrix of the whole system |
| $k_{\text{eq}}$ | = | equivalent stiffness |
| $k_0$ | = | stiffness of the MR damper |
| $\boldsymbol{M}$ | = | global mass matrix of the whole system |
| $m_{\text{eq}}$ | = | equivalent mass |
| $m_{\text{MR}}$ | = | mass of the MR damper |
| $\boldsymbol{R}$ | = | transformation matrix |
| $\boldsymbol{W}$ | = | diagonal penalty weighting matrix |
| $z$ | = | evolutionary shape variable |
| $\alpha, B, G, A$ | = | characteristic parameters in Bouc–Wen model |
| $\beta, \gamma$ | = | controlling parameters in Newmark's method |
| $\boldsymbol{\Phi}$ | = | modal matrix |
| $\{\boldsymbol{F}_z\}$ | = | vector of hysteresis or evolutionary force |

## I. Introduction

THE design of mechanical systems with reduced response to vibrations based on semi-active damping has been a challenging task. The emerging of new multifunctional materials and devices along with the evolution of computers and design optimization algorithms have provided new tools to be applied in the reduction of vibration in structural systems. Among these new tools, the Magnetorheological (MR) dampers have recently shown some promises in semi-active vibration control applications. Their mechanical simplicity, high dynamic range, lower power requirements, large force capacity, and robustness are some of the characteristics of the MR dampers that have attracted the attention of researchers in recent years. These dampers use magnetorheological fluids that are sensible to changing of the magnetic fields and offer rapid variation in damping properties in a reliable fail-safe manner. MR dampers are very efficient to semiactively control vibration in many applications such as civil, aerospace, and automotive engineering.

Among the models proposed to simulate the hysteresis behavior of MR dampers, the Bouc–Wen model [1,2] has been extensively used. Spencer et al. [3] proposed a phenomenological model for MR dampers based on the Bouc–Wen hysteresis model. This model is able to capture the force rolloff in the low velocity region that is observed in the experimental data. Yang et al. [4] proposed a phenomenological model which considers the MR fluid adhesive phenomenon, as well as inertial and shear thinning effects. To accomplish this, they modified the damping constant in the Bouc–Wen model by a monotonically decreasing function with respect to absolute velocity. Choi and Lee [5] have developed a polynomial model that includes the excitation current as variable. Wang et al. [6] proposed the equivalent characteristic method, which considers the relationships between the hysteresis phenomenon and the frequency and stroke of the excitation as well as the current excitation. Recently, Dominguez et al. [7] proposed a model based on the Bouc–Wen model that employs the current, frequency, and amplitude excitation as inputs.

Several types of semi-active vibration suppression have been proposed and studied. Onoda et al. [8] designed and fabricated a variable damper using electro-rheological (ER) fluid and proposed a semi-active control scheme base on the linear quadratic regulator (LQR) control theory. Dyke et al. [9] presented the clipped linear optimal control law that has been shown to be effective for MR damper. Soong and Spencer [10] provided an updated current development and structural applications of active structural control. The application of hybrid mass dampers in tall buildings has been studied for different semi-active controls [11–13]. A semi-active optimal control method for nonlinear multi-degree-of-freedom

Received 24 June 2005; revision received 5 January 2006; accepted for publication 10 January 2006. 

*Assistant professor, Faculty of Engineering; auredgz@uaq.mx.
†Assistant professor, Department of Mechanical Engineering and Industrial Engineering; sedagha@alcor.concordia.ca. Member AIAA.
‡Associate professor, Department of Mechanical Engineering and Industrial Engineering; istih@vax2.concordia.ca.

systems using magnetorheological-tuned liquid column dampers under random wind excitation in tall buildings was performed by Ying et al. [14]. Zhu et al. [15] used the Bingham model to predict the forces of the MR/ER dampers and determined an optimal control law by using the stochastic dynamical programming principle.

In this study the feature and simulation of the hysteresis behavior of the MR damper have been briefly explained. Then the finite element formulation of the adaptive space truss structure with integrated MR damper is presented. This is followed by the solution for the nonlinear system using Newmark method with inner iterative process. The simulation results of the nonlinear model of the structure are validated with experimental data. Finally, a vibration suppression strategy is proposed and applied to the structure. A local and global vibration performance index was applied to evaluate the vibration reduction achieved with the proposed strategy. A significant reduction in both local and global vibration of the structure has been observed.

## II. Model of the MR Damper

MR dampers are semi-active devices that use MR fluids to construct a versatile damping device. The MR damper typically consists of a hydraulic cylinder that contains micrometer-sized magnetically polarizeable particles dispersed in mineral oil. When the particles are polarized under the presence of magnetic fields, the MR fluid offers a high resistance to flow. Given that the strength of the magnetic field controls the yield stress of the fluid, devices utilizing MR fluid are expected to be performant for a wide range of situations. The schematic representation of the cylindrical type of MR damper is shown in Fig. 1. In this kind of damper, the MR fluid inside the cylinder flows through the MR valve, which is a fixed-size orifice on the piston. The magnetic field generated by electromagnet yields a change in viscosity of the MR fluid, causing a pressure differential for the flow of fluid passing through the valve. The pressure differential is directly proportional to the force required to move the damper rod. As such, the damping characteristic of the MR damper is a function of the magnetic field (or electrical current). This relationship allows the damping characteristic of the MR damper to be easily controlled in real time.

The Bouc–Wen is a suitable dynamic model that has been extensively applied to simulate the hysteresis behavior experienced by MR dampers, as it possesses the force-displacement and force-velocity behavior, which resembles that of the real life MR dampers. The Bouc–Wen model is illustrated in Fig. 2.

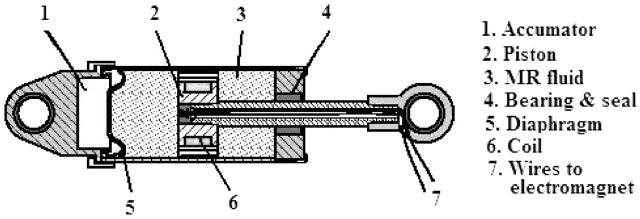


**Fig. 1 Functional configuration of a MR damper.**

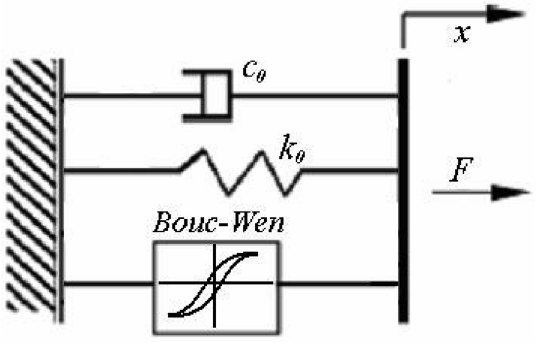


**Fig. 2 Bouc–Wen model.**

The corresponding mathematical representation of the damping force in the Bouc–Wen model can be expressed as

$$F[x(\tau), \dot{x}(\tau), 0 \le \tau \le t; t] = c_0\dot{x} + k_0 x + \alpha z \tag{1}$$

where $z$ is described by the first order differential equation as follows:

$$\dot{z} = -G|\dot{x}||z|^{(n-1)}z - B\dot{x}|z|^n + A\dot{x} \tag{2}$$

The parameters $c_0$, $k_0$, $\alpha$, $B$, $G$, $n$ and $A$ are called characteristic parameters of the Bouc–Wen model which can control the linearity and the smoothness of the transition from the preyield to the postyield region.

One of the major problems in the Bouc–Wen model is the accurate determination of its characteristic shape parameters. In other words, the characteristic parameters of the Bouc–Wen model should be determined such that to accurately characterize the hysteresis phenomenon of MR dampers. Usually an optimization technique is applied to find these parameters of such a manner that the error between experimental and simulation results be minimized; however, this approach is computationally expensive and still some differences between the model and the experimental data exist. To alleviate this problem, a methodology was developed by Dominguez et al. [16] to find the characteristic parameters of the Bouc–Wen model in the attempt to better characterize the hysteresis phenomenon of the MR damper. The methodology employs key information from the experimental data to find directly the value of the characteristic parameters and avoids applying any optimization method to match the experimental curves, thus eliminating errors and high computational costs inherent in the optimization procedure.

The results of the proposed methodology suggest that linear and exponential relations exist between the characteristic parameters and the current excitation. Furthermore, parabolic relations were found between the frequency and amplitude excitations and the hysteresis force. All these relations were incorporated into a new dynamic model [7] based on the Bouc–Wen model to predict the damping force as

$$\begin{aligned} &F[x(\tau), \dot{x}(\tau), I, \omega, x, 0 \le \tau \le t; t] \\ &\quad = (d_1\omega^{d_2})(d_3 x_{\max}^{d_4})[c_0(I)\dot{x} + k_0(I)x + \alpha(I)z] \end{aligned} \tag{3}$$

where $\omega$ is the frequency of the excitation, $d_1, \ldots, d_4$ are constants and $z$ is defined by the following differential equation:

$$\dot{z}(I) = G(I)|\dot{x}||z|^{(n-1)}z - B(I)\dot{x}|z|^n + A(I)\dot{x} \tag{4}$$

where $A$ and $B$ are assumed to be one and zero, respectively, and

$$\begin{aligned} c_0(I) &= c_1 + c_2[1 - e^{-c_3(I-I_c)}] \quad \text{for } I > I_c \\ c_0(I) &= c_4 + \tfrac{c_4 - c_1}{I_c} I \quad \text{for } I \le I_c \end{aligned} \tag{5}$$

$$k_0(I) = k_1 + k_2 I \tag{6}$$

$$\begin{aligned} \alpha(I) &= \alpha_1 + \alpha_2[1 - e^{-\alpha_3(I-I_c)}] \quad \text{for } I > I_c \\ \alpha(I) &= \alpha_1 + \tfrac{\alpha_4 - \alpha_1}{I_c} I \quad \text{for } I \le I_c \end{aligned} \tag{7}$$

$$G(I) = \gamma_1 - \gamma_2 I \tag{8}$$

$$\begin{aligned} F_{z0}(I) &= F_{z01} + F_{z02}[1 - e^{-F_{z03}(I-I_c)}] \quad \text{for } I > I_c \\ F_{z0}(I) &= F_{z04} + \tfrac{F_{z04} - F_{z01}}{I_c} I \quad \text{for } I > I_c \end{aligned} \tag{9}$$

where 16 constant parameters, $c_1, c_2, c_3, c_4, k_1, k_2, \alpha_1, \alpha_2, \alpha_3, \alpha_4, \gamma_1, \gamma_2$, $F_{z01}$, $F_{z02}$, $F_{z03}$, and $F_{z04}$, relate the characteristic shape parameters to current excitation and should be specified in a way to better characterize the behavior of the MR dampers. $I_c$ is the critical current in which the characteristic parameters change their linear behavior in low velocity to exponential behavior in high velocity.

Now using these current dependent parameters, the solution of the evolutionary variable may be written as the following form [7]:

$$z(I) = \frac{1}{\sqrt{G(I)}} \tanh\left\{ \sqrt{G(I)}\left[ \dot{x} + \frac{1}{\sqrt{G(I)}} a \tanh\left( \frac{F_{z0}(I)\sqrt{\gamma(I)}}{\alpha(I)} \right) \right] \right\} \quad \text{for} \begin{cases} (z<0, x<0) & \text{or} \\ (z \geq 0, x<0) \end{cases} \tag{10}$$

$$z(I) = \frac{1}{\sqrt{G(I)}} \tanh\left\{ \sqrt{G(I)}\left[ \dot{x} + \frac{1}{\sqrt{G(I)}} a \tanh\left( \frac{F_{z0}(I)\sqrt{\gamma(I)}}{\alpha(I)} \right) \right] \right\} \quad \text{for} \begin{cases} (z \geq 0, x \geq 0) & \text{or} \\ (z<0, x \geq 0) \end{cases} \tag{11}$$

It is noted that in this new model, the characteristic parameters are a function of the current, frequency, and amplitude excitation. Thus the hysteresis force of the MR damper can be easily evaluated for any desired combination of the frequency, amplitude, and current excitations without any revaluation of these characteristics parameters. This is not the case for the simple or traditional Bouc–Wen model in which the characteristic parameters are valid only for a specific excitation.

The ability of the proposed model to predict the hysteresis force for any excitation condition can make it instrumental for the semi-active control applications.

## III. Finite Element Formulation

Discrete structures may require some connecting parts (representing nodes and bolts) to assemble the elements of the structure. These parts usually have different mechanical properties and dimensions that should be considered in the finite element formulation of the structure. Considering this, a finite element model that accurately describes the behavior of the bar and connecting elements is required. For this purpose, a bar element containing three members as shown in Fig. 3 is developed. The element is shown in its local coordinates with end nodes N1 and N2. It is noted that the middle member of the element, E2, represents the structural element (hollow cylinder in this study) for which the physical characteristics are known and the adjacent members E1 and E3 are the connecting elements.

As the elements are in series the equivalent stiffness and mass of the proposed bar can be calculated by

$$k_{\text{eq}} = \frac{k_1 k_2 + k_1 k_3 + k_2 k_3}{k_1 k_2 k_3}; \qquad m_{\text{eq}} = m_1 + m_2 + m_3 \tag{12}$$

Considering this, the stiffness and lumped mass matrices for the complete bar element in local coordinates may be described as

$$[\boldsymbol{K}_{\text{eq}}^{(e)}] = \begin{bmatrix} k_{\text{eq}} & -k_{\text{eq}} \\ -k_{\text{eq}} & k_{\text{eq}} \end{bmatrix}; \qquad [\boldsymbol{M}_{\text{eq}}^{(e)}] = \begin{bmatrix} \frac{m_{\text{eq}}}{2} & 0 \\ 0 & \frac{m_{\text{eq}}}{2} \end{bmatrix} \tag{13}$$

The local elemental stiffness and mass matrices can be transformed to the global coordinates using the rotational or transformation matrix for truss elements [17] as

$$[\boldsymbol{K}]^g = [\boldsymbol{R}]^T [\boldsymbol{K}_{\text{eq}}^{(e)}][\boldsymbol{R}]; \qquad [\boldsymbol{M}]^g = [\boldsymbol{R}]^T [\boldsymbol{M}_{\text{eq}}^{(e)}][\boldsymbol{R}] \tag{14}$$

Once the transformation has been performed, the matrices can be assembled properly to obtain the system stiffness and mass matrices. Using the proportional damping [18], the global damping matrix can also be obtained as

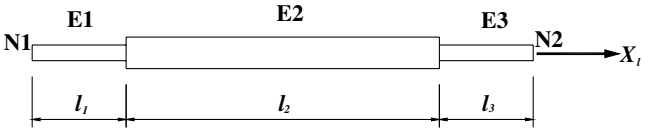


**Fig. 3 Finite element of a passive bar element.**

$$[\boldsymbol{C}] = 2[\boldsymbol{\Phi}]^{-T}[\boldsymbol{\Omega}][\boldsymbol{\zeta}][\boldsymbol{\Phi}]^{-1} \tag{15}$$

where the diagonal eigenvalue matrix $[\boldsymbol{\Omega}]$ and the damping ratio matrix $[\boldsymbol{\zeta}]$ are specified as

$$[\boldsymbol{\Omega}]^2 = \begin{bmatrix} \omega_1^2 & 0 & \cdots & 0 \\ 0 & \omega_n^2 & \cdots & 0 \\ \vdots & \vdots & \ddots & \vdots \\ 0 & 0 & \cdots & \omega_n^2 \end{bmatrix}; \qquad [\boldsymbol{\zeta}] = \begin{bmatrix} \zeta_1 & 0 & \cdots & 0 \\ 0 & \zeta_2 & \cdots & 0 \\ \vdots & \vdots & \ddots & \vdots \\ 0 & 0 & \cdots & \zeta_n \end{bmatrix} \tag{16}$$

Now assuming that the mass of the MR damper can be equally lumped at both ends, the finite element model for the MR damper is obtained by applying the Second Newton's Law to the masses shown in Fig. 4:

$$\begin{cases} c_0(\dot{\boldsymbol{x}}_j - \dot{\boldsymbol{x}}_i) + k_0(\boldsymbol{x}_j - \boldsymbol{x}_i) + \alpha z - \boldsymbol{F}_0 = \frac{m_{\text{MR}}}{2} & \ddot{x}_i \\ c_0(\dot{\boldsymbol{x}}_i - \dot{\boldsymbol{x}}_j) + k_0(\boldsymbol{x}_i - \boldsymbol{x}_j) - \alpha z + \boldsymbol{F}_0 = \frac{m_{\text{MR}}}{2} & \ddot{x}_j \end{cases} \tag{17}$$

where $k_0$ is the time dependent stiffness mainly due to the effect of gas accumulator in the MR damper, $c_0$ is the time dependent viscous damping coefficient, $\alpha z$ is the evolutionary force and $\boldsymbol{F}_0$ is the initial force required to install the MR damper in its initial position.

Writing Eqs. (17) in the matrix form yields:

$$\begin{aligned} &\begin{bmatrix} \frac{m_{\text{MR}}}{2} & 0 \\ 0 & \frac{m_{\text{MR}}}{2} \end{bmatrix} \begin{Bmatrix} \ddot{x}_i \\ \ddot{x}_j \end{Bmatrix} + \begin{bmatrix} c_0 & -c_0 \\ -c_0 & c_0 \end{bmatrix} \begin{Bmatrix} \dot{x}_i \\ \dot{x}_j \end{Bmatrix} \\ &\quad + \begin{bmatrix} k_0 & -k_0 \\ -k_0 & k_0 \end{bmatrix} \begin{Bmatrix} x_i \\ x_j \end{Bmatrix} \\ &\quad = \begin{bmatrix} 1 & 0 \\ 0 & 1 \end{bmatrix} \begin{Bmatrix} \alpha z \\ -\alpha z \end{Bmatrix} + \begin{bmatrix} 1 & 0 \\ 0 & 1 \end{bmatrix} \begin{Bmatrix} -\boldsymbol{F}_0 \\ \boldsymbol{F}_0 \end{Bmatrix} \end{aligned} \tag{18}$$

or

$$[\boldsymbol{M}_{\text{MR}}]\{\ddot{\boldsymbol{x}}\} + [\boldsymbol{C}_0]\{\dot{\boldsymbol{x}}\} + [\boldsymbol{K}_0]\{\boldsymbol{x}\} = [\boldsymbol{I}]\{\boldsymbol{F}_z\} + [\boldsymbol{I}]\{\boldsymbol{F}_0\} \tag{19}$$

where $\{\boldsymbol{x}\}$, $\{\dot{\boldsymbol{x}}\}$ and $\{\ddot{\boldsymbol{x}}\}$ are the vectors of nodal displacement, velocity, and acceleration for the MR damper, respectively. $[\boldsymbol{M}_{\text{MR}}]$, $[\boldsymbol{C}_0]$ and $[\boldsymbol{K}_0]$ are the lumped mass, damping and stiffness matrices, respectively, and $\{\boldsymbol{F}_z\}$ and $\{\boldsymbol{F}_0\}$ are the vector of hysteresis and initial forces, respectively.

Similarly, the mass and stiffness matrices of the MR damper can be transformed to global coordinates for assembling purposes. It is noted that the damping coefficient is significantly larger than the

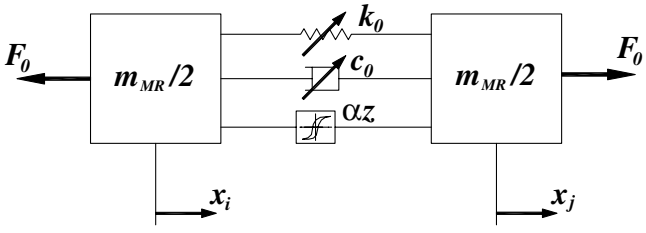


**Fig. 4 Lumped mass representation of the MR damper.**

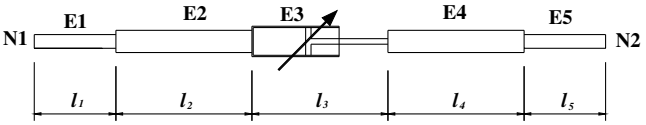


**Fig. 5 Finite element for the MR damper bar element.**

typical structural damping of the bars; thus, the structural damping may be ignored. The global damping matrix of the bar element with MR damper can also be obtained by transforming the local damping matrix using the rotational matrix as

$$[\boldsymbol{C}_0]^g = [\boldsymbol{R}]^T[\boldsymbol{C}^{(e)}][\boldsymbol{R}] \tag{20}$$

It is noted that the global damping matrix $[\boldsymbol{C}_0]^g$ is the matrix with time dependent coefficients.

In designed space truss structure, the MR damper replaces part of a member of the truss structure. Here, this active member is modeled as shown in Fig. 5. The middle element E3 represents the MR damper. The end elements, E1 and E5, simulates the node and bolt connections and the elements E2 and E4 are the bar members to connect the MR damper to the Elements E1 and E5.

As the elements shown in Fig. 5 are in series, the equivalent stiffness and mass matrices can be easily obtained as

$$k_{\text{eq}} = \frac{k_1k_2k_0k_4k_5}{k_2k_0k_4k_5 + k_1k_0k_4k_5 + k_1k_2k_4k_5 + k_1k_2k_0k_5 + k_1k_2k_0k_4}$$
$$m_{\text{eq}} = m_1 + m_2 + m_{\text{MR}} + m_4 + m_5 \tag{21}$$

Finally the stiffness and mass matrices for the members with MR damper are obtained by substituting the equivalent stiffness and mass matrices given in Eq. (21) into Eqs. (13) and (14). It should be noted that the stiffness and damping matrices for the MR damper bar element have time dependent coefficients due to inherent nonlinearity of the controllable damper. The final matrix formulation of the adaptive structure can be stated as

$$[\boldsymbol{M}]\{\ddot{\boldsymbol{x}}(t)\} + [\boldsymbol{C}(t)]\{\dot{\boldsymbol{x}}(t)\} + [\boldsymbol{K}(t)]\{\boldsymbol{x}(t)\} = \{\boldsymbol{F}(t)\} \tag{22}$$

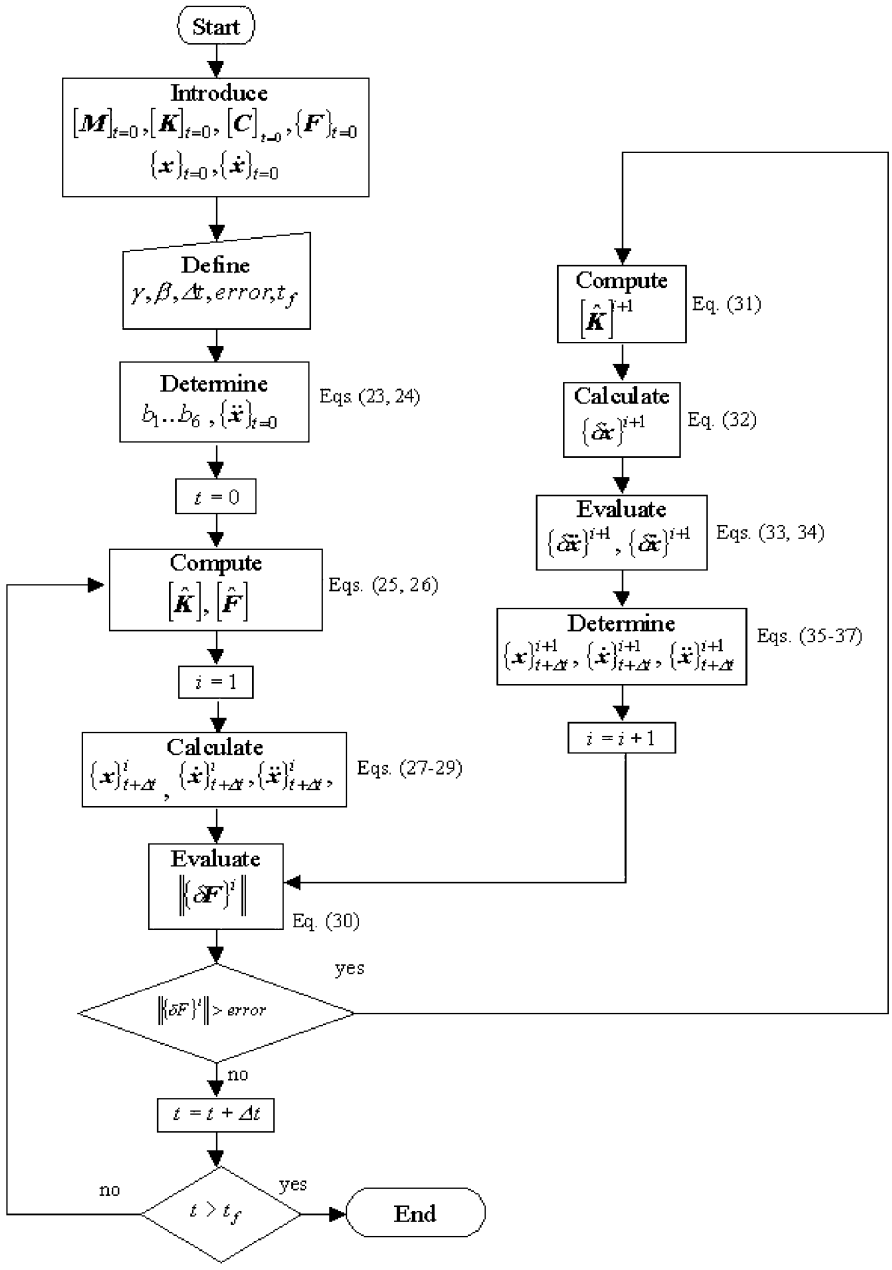


**Fig. 6 Newmark's method with inner iterative process.**

## IV. Solution of the Governing Equations

To solve the governing differential equations in (22), the powerful Newmark $\beta$ method [18] is applied with an inner iterative process to maintain the equilibrium of the forces at each time step. The Newmark method is a single step integration implicit method that attempts to satisfy the differential equation of motion at time $t + \Delta t$ after the solution at time $t$ is found. The modified Newmark method with an inner iterative process is formulated as follows:

$$b_1 = \frac{1}{\beta \Delta t^2}; \qquad b_2 = \frac{1}{\beta \Delta t}; \qquad b_3 = \beta - \frac{1}{2}$$
$$b_4 = \gamma \Delta t b_1; \qquad b_5 = 1 + \gamma \Delta t b_2; \qquad b_6 = \Delta t(1 + \gamma b_3 - \gamma) \tag{23}$$

$$\{\ddot{\boldsymbol{x}}\}_t = [\boldsymbol{M}]^{-1}(\{\boldsymbol{F}\}_t - [\boldsymbol{C}]\{\dot{\boldsymbol{x}}\}_t - [\boldsymbol{K}]\{\boldsymbol{x}\}_t \tag{24}$$

$$[\hat{\boldsymbol{K}}] = b_1[\boldsymbol{M}] + b_4[\boldsymbol{C}] + [\boldsymbol{K}] \tag{25}$$

$$\{\boldsymbol{F}\} = \{\boldsymbol{F}\}_{t+\Delta t} + [\boldsymbol{M}](b_1\{\boldsymbol{x}\}_t + b_2\{\dot{\boldsymbol{x}}\}_t + b_3\{\ddot{\boldsymbol{x}}\}_t) + [\boldsymbol{C}](b_4\{\boldsymbol{x}\}_t + b_5\{\dot{\boldsymbol{x}}\}_t + b_6\{\ddot{\boldsymbol{x}}\}_t) \tag{26}$$

$$\{\boldsymbol{x}\}_{t+\Delta t} = [\hat{\boldsymbol{K}}]^{-1}\{\hat{\boldsymbol{F}}\} \tag{27}$$

$$\{\dot{\boldsymbol{x}}\}_{t+\Delta t} = b_4(\{\boldsymbol{x}\}_{t+\Delta t} - \{\boldsymbol{x}\}_t) + b_5\{\dot{\boldsymbol{x}}\}_t + b_6\{\ddot{\boldsymbol{x}}\}_t \tag{28}$$

$$\{\ddot{\boldsymbol{x}}\}_{t+\Delta t} = b_1(\{\boldsymbol{x}\}_{t+\Delta t} - \{\boldsymbol{x}\}_t) + b_2\{\dot{\boldsymbol{x}}\}_t + b_3\{\ddot{\boldsymbol{x}}\}_t \tag{29}$$

$$\{\delta \boldsymbol{F}\}^i = \{\boldsymbol{F}\}_{t+\Delta t} + [\boldsymbol{M}]\{\ddot{\boldsymbol{x}}\}^i_{t+\Delta t} - [\boldsymbol{C}]^i_{t+\Delta t}\{\dot{\boldsymbol{x}}\}^i_{t+\Delta t} - [\boldsymbol{K}]^i_{t+\Delta t}\{\boldsymbol{x}\}^i_{t+\Delta t} \tag{30}$$

$$[\hat{\boldsymbol{K}}]^{i+1} = [\boldsymbol{K}]^i_{t+\Delta t} + b_1[\boldsymbol{M}] + b_4[\boldsymbol{C}]^i_{t+\Delta t} \tag{31}$$

$$\{\delta \boldsymbol{x}\}^{i+1} = [\hat{\boldsymbol{K}}]^{-1,i+1}\{\delta \boldsymbol{F}\}^i \tag{32}$$

$$\{\delta \dot{\boldsymbol{x}}\}^{i+1} = b_4\{\delta \boldsymbol{x}\}^{i+1} \tag{33}$$

$$\{\delta \ddot{\boldsymbol{x}}\}^{i+1} = b_1\{\delta \boldsymbol{x}\}^{i+1} \tag{34}$$

$$\{\boldsymbol{x}\}^{i+1}_{t+\Delta t} = \{\delta \boldsymbol{x}\}^{i+1} + \{\boldsymbol{x}\}^i_{t+\Delta t} \tag{35}$$

$$\{\dot{\boldsymbol{x}}\}^{i+1}_{t+\Delta t} = \{\delta \dot{\boldsymbol{x}}\}^{i+1} + \{\dot{\boldsymbol{x}}\}^i_{t+\Delta t} \tag{36}$$

$$\{\ddot{\boldsymbol{x}}\}^{i+1}_{t+\Delta t} = \{\delta \ddot{\boldsymbol{x}}\}^{i+1} + \{\ddot{\boldsymbol{x}}\}^i_{t+\Delta t} \tag{37}$$

The flowchart of the solution finding process is also shown in Fig. 6.

## V. Description of the Experiment

The finite element model of the adaptive space truss was experimentally validated with an aluminum discrete space structure that was assembled. Figure 7 illustrates the complete geometric configuration of the test specimen with the associated node numbers and experimental setup. The test specimen consists of a four-bay space truss structure. Each assembled bay is a 0.707 m cube shaped structure. The lumped mass of 1.44 kg has been attached to the free nodes 3, 4, 7, 8, and 9–12, and the lumped mass of 2.88 kg to the free nodes of 13–20. The nodes 1, 2, 5, and 6 are fixed to the shaker.

Two accelerometers were properly set and calibrated to measure the input and output accelerations. The first accelerometer (input) is mounted on the plate that supports the structure and the second (output) is located on the structure at node 19. The signals from accelerometers are amplified and then fed into the signal analyzer

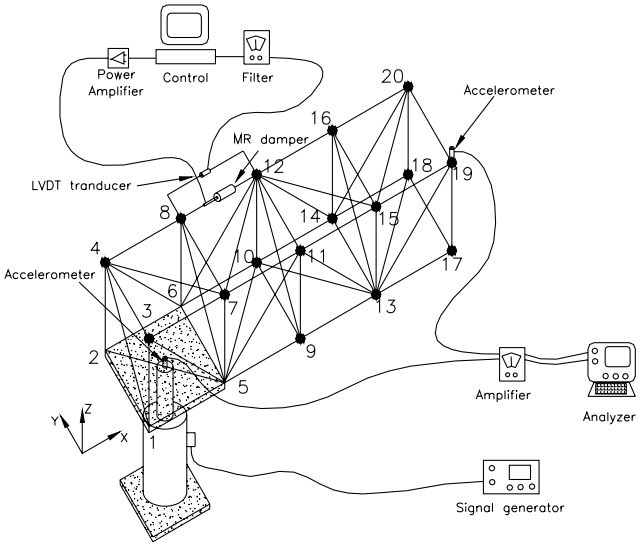


**Fig. 7 Schematic setup of the test.**

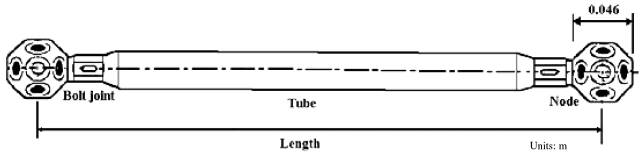


**Fig. 8 Typical assembly of a bar element.**

unit to obtain the transmissibility spectrum in the frequency domain. The MR damper model RD-1005-3 manufactured by Lord Corporation has been embedded into the structure between the nodes 8 and 12. This is a compact MR damper with mass of 0.8 kg which can be applicable to an adaptive space truss structures or other medium load requirement application such as a middle-sized passenger suspended seat in heavy vehicles. The compressed length and extended length of the damper are 0.155 and 0.208 m, respectively. The body and shaft diameters are also 0.414 and 0.010 m, respectively. A DC maximum current of 2 A is used as command signal as well as the input for the coils 9 (it is noted that the MR damper is operated during the experiment with maximum current 1.5 A for the sake of safety). The electric resistance of the coil varies from 5 $\Omega$, at ambient temperature to 7 $\Omega$, at 70°C, and for an input voltage of 12 V DC.

The relative velocity between two ends of the MR damper is obtained by the linear velocity transducer sensor which is installed in parallel with the MR damper. The output signal from the control is fed into a power amplifier circuit to provide the controlled current excitation (maximum current value is 1.5 A) to the MR damper.

Bar elements are aluminum pipes and those elements located in $X$, $Y$, and $Z$ directions have dimensions of $0.707 \times 0.030 \times 0.015$ m for the outside diameter, inside diameter, and thickness, respectively. The dimensions for the diagonal members are $1.000 \times 0.022 \times 0.001$ m. The connection node has a mass of 0.08 kg and is bolt connected with the bar members. Figure 8 shows a typical assembly of a bar element used to fabricate the test article and consists of a pipe with bolt connected nodes.

## VI. Semi-active Vibration Control Strategy

Semi-active devices can control the state of systems such that their inherent damping characteristics are enhanced. Using semi-active approach, vibration is suppressed by passive energy dissipation mechanisms. Therefore, systems are always stable even with improper selection of the control logic due to, for example, lack of exact information about the dynamic characteristics of the structure.

There have been investigated different kinds of control strategies for semi-active dampers. The continuous strategies, although maybe

more effective, might also come with some drawbacks, such as the approach might require considerable computational time for many degrees of freedom structural systems to determine the more appropriate control current, and, despite the lengthy computation time, it may be possible for the inherent hysteretic behavior of the MR damper to adversely influence the performance of the overall system. The ON-OFF strategy has been proven effective for systems involving inherent hysteresis. The capability to vary the current is definitely an asset that is worthwhile to investigate. The proposed ON-OFF control strategy employs the absolute velocity at the end of the MR damper in local coordinates and the hysteresis force experienced by the MR damper. It assigns maximum current when the both velocity and hysteresis force have the same sign and zero when the sign of both is different. The proposed strategy can be mathematically stated as

$$\begin{cases} I_{\max} & \text{when } \dot{x}_j F_z > 0 \\ I_{\min} & \text{when } \dot{x}_j F_z \le 0 \end{cases} \tag{38}$$

## VII. Simulation and Experimental Results

In this section the proposed finite element model for the adaptive space truss structure with embedded MR damper is validated using experimental results. Further, the proposed vibration suppression strategy has been used to reduce the structural vibration.

As discussed, the model for the MR damper bar consists of five elements and the passive bar contains three elements. The connecting elements E1 and E3 in Fig. 3 have outside diameter, thickness, and length of 0.011, 0.00035, and 0.064 m, respectively. Similar values are considered for the elements E1 and E5 of Fig. 5. The E2 and E4 are solid bars of aluminum with diameter of 0.012 m and length of 0.181 and 0.200 m, respectively. The MR damper was installed in the middle position as E3 in Fig. 5; thus, an initial compressed force is considered in the model. The MR damper model RD-1005-3 manufactured by Lord Corporation has been characterized [7], and the values of the constant parameters are: $c_1 = 358$ Ns/m, $c_2 = 280$ Ns/m, $c_3 = 2.4$ A$^{-1}$, $c_4 = 230$ Ns/m, $k_1 = 1085$ N/m, $k_2 = 2928$ N/A $\cdot$ m, $\alpha_1 = 1514$ N/m, $\alpha_2 = 4200$ N/m, $\alpha_3 = 2.2$ A$^{-1}$, $\alpha_4 = 82$ N/m, $\gamma_1 = 280$ m$^{-2}$, $\gamma_2 = 8.66$ m$^{-2}$ A$^{-1}$, $d_1 = 5.08$ m, $d_2 = 0.333$, $d_3 = 0.251$ s/rad, $d_4 = 0.351$, $F_{z01} = 67$ N, $F_{z02} = 250$ N, $F_{z03} = 1.9$ A$^{-1}$, and $F_{z04} = 1.32$ N.

The proportional damping approach has been used to determine the damping matrix. A structural damping ratio of 1.6% is considered for all the modes of vibration to match the transmissibility amplitude of the model with the experimental data. The natural frequencies of the structural are well separated and the effect of the higher modes in the response of the system is found to be negligible. The Newmark method explained in Sec. IV was applied to obtain the transient response with time increment of 0.004 s. The control parameters are selected as $\beta = 0.25$ and $\gamma = 0.5$ to have unconditional numerical stability. Using the information obtained from instant displacement $x$, velocity $\dot{x}$, and acceleration $\ddot{x}$, the instant maximum velocity is approximated as [6]

$$\dot{x}_{\max} = \sqrt{\dot{x}^2 + x\ddot{x}} \tag{39}$$

Using Eq. (39) the maximum displacement can be obtained as

$$x_{\max} = \dot{x}_{\max}/\omega \tag{40}$$

where $\omega$ represents the fundamental natural frequency for transient problems.

Figure 9a shows the comparison of the transient response (acceleration in $Z$-direction at node 19) between the test and the simulation without using the MR damper. In this experiment the structure is base excited along $Z$-direction with a step function of amplitude 0.0254 m and then released until it reaches the equilibrium point. The MR damper is then installed between nodes 8 and 12 with maximum current excitation of 1.5 A and the same experiment has been conducted. The result is shown in Fig. 9b. A reasonable agreement exists between simulation and experimental results. Also it can be seen that the vibration performance of the structure has been significantly improved by installing MR damper under current excitation of 1.5 A. As it can be observed, there is very good agreement not only in the amplitude but also in the frequency at the beginning between the simulation results and the experimental data; however, some differences are observed at the end of the simulation. This is mainly due to the use of proportional damping, which rapidly damps out the higher natural modes. It is also noted that the fundamental natural frequency of the structure without MR damper is found to be 9.10 Hz numerically and 8.8 Hz experimentally (the error is less than 4%). Thus this finite element formulation predicts, in this case, the response of the structural system and may be used with confidence for vibration control, which is the main objective of this paper.

It has also been found that the fundamental natural frequency of the structure increases insignificantly from 9.10 Hz when the MR damper is not installed to 9.13 Hz, when the MR damper is installed without current excitation. The fundamental natural frequency of the structure with embedded MR damper increases as the current excitation increases. The fundamental natural frequencies are found to be 10.06 and 10.38 Hz for 0.75 and 1.5 A, respectively.

Now, the proposed strategy to suppress the vibration in the test article is applied. To measure the effectiveness of the MR damper in vibration control applications, a performance index function has been defined. The following displacement part of performance index which is frequently used in LQR control has been employed [19]:

$$f(\boldsymbol{x}, t) = \int_{t_0}^{t_f} \{\boldsymbol{x}\}^T [\boldsymbol{W}] \{\boldsymbol{x}\} \, \mathrm{d}t \tag{41}$$

This performance index may be applied to measure the global vibration of the whole structure if all the components of the displacement vector $\{\boldsymbol{x}\}$ are considered or to measure the local vibration if only the components of the desired nodal displacement are considered. Here, both global and local vibrations are evaluated and compared. It should be mentioned that it is logical to think that the mass of the MR damper could affect the response of the system.

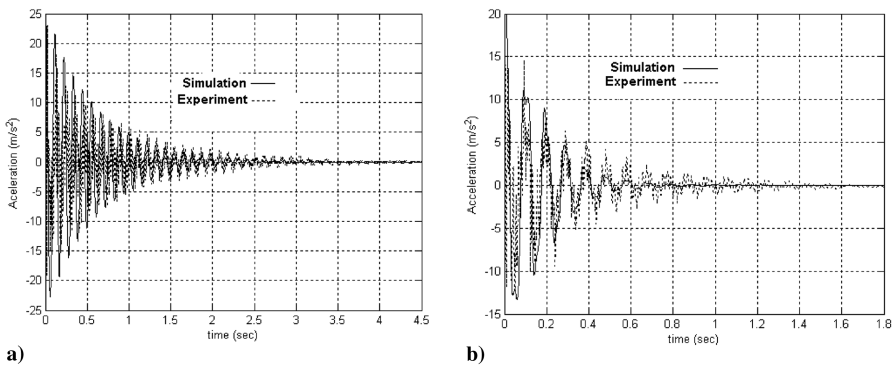


**Fig. 9 a) $Z$-acceleration response at node 19 of passive structure under step base excitation; b) $Z$-acceleration response at node 19 (with MR damper installed and 1.5 A).**

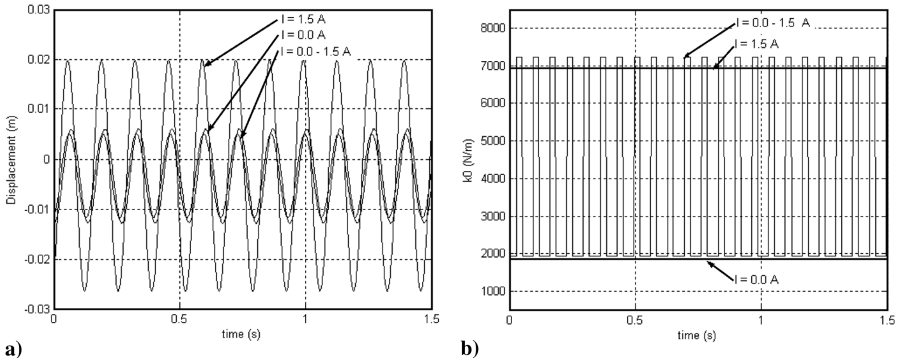


a) b)

**Fig. 10 a) Absolute *Z*-displacement of node 19 under harmonic base excitation; b) MR damper stiffness variation under harmonic base excitation.**

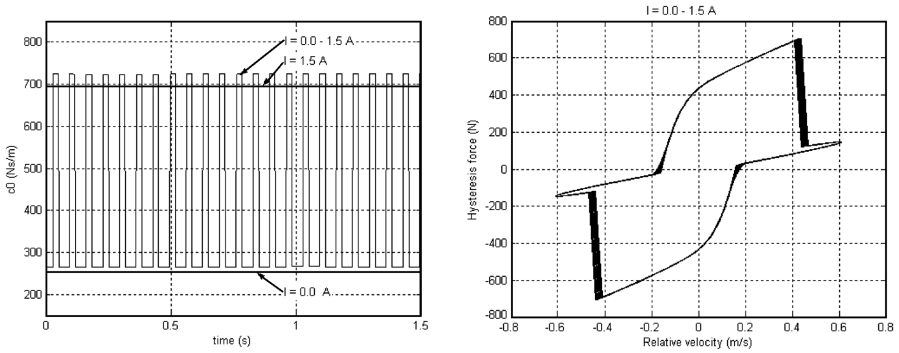


a) b)

**Fig. 11 a) MR damper damping coefficient variation under harmonic base excitation; b) Hysteresis force in MR damper under harmonic excitation using semi-active vibration control.**

However, in this study, the effect of mass of damper on structural response was found to be negligible and the response is mainly affected by changing the damping and the inherent stiffness of the MR damper. Furthermore, the mass of the MR damper has been considered in the finite element formulation of the semi-active bar. Considering this, in the performance index function, no penalty due to the increase of mass to the structure has been considered.

Different simulations are carried out to validate the proposed strategy. Here the MR damper is installed between the nodes 6 and 10. The simulations were performed using the Newmark method with time increment of 0.0015 s. The absolute *Z*-displacement response of node 19 has been obtained for three different cases: 1) applying proposed semi-active vibration control strategy ($I = 0.0 - 1.5$ A) given in Eq. (38), 2) applying $I = 0.0$ A to the MR damper, and 3) applying $I = 1.5$ A constant current to the MR damper. First, the responses of the structure under harmonic base excitation with amplitude and frequency excitation of 0.0127 m and 7.5 Hz, respectively, are compared for the preceding cases in Fig. 10a. The variation of MR damper stiffness and damping coefficient with and without proposed semi-active vibration control strategy is demonstrated in Figs. 10b and 11a, respectively. As it can be realized using the proposed strategy, the vibrations have been drastically reduced. The hysteresis force loops with and without proposed vibration control strategy for the case of harmonic excitation are also shown in Fig. 11b. The value of the performance index function for each case of excitation current is evaluated using Eq. (41) for local (node 19) and global vibration with $t_0 = 0$ and $t_f = 1.5$ s and is provided in Table 1.

Next the transient response of the structure for the aforementioned three cases is investigated. The structure is excited at its base with the step input of 0.0254 m. The absolute *Z*-response of node 19 for the three cases is shown in Fig. 12a. The variation of the MR damper stiffness and damping coefficient are also shown in Figs. 12b and 13a, respectively, and the hysteresis loop for transient response with the proposed strategy is shown in Figs. 13b. The performance index function for with and without proposed vibration suppression strategy under transient excitation is evaluated using Eq. (41) and presented in Table 1. It should be noted that the global and local vibration (node 19) were obtained for a period of 2 s of the transient response.

Finally the structure is excited at its base with the random vibration shown in Fig. 14a. The responses of the structure, when constant current excitations of 0.0 and 1.5 A are applied to the MR damper, are compared with those obtained with the proposed vibration control strategy and shown in Fig. 14b. The relative displacement between both ends of the MR damper using the proposed strategy is also presented in Fig. 15a and its correspondent hysteresis force experienced by the MR damper can be seen in Fig. 15b. Figures 16a and 16b illustrate the variations of the damping and stiffness coefficients using the proposed control strategy under random excitation. The quantitative comparison is also evaluated using the performance index function in Eq. (41) and is presented in Table 1 for local (node 19) and global vibration with $t_0 = 0$ and $t_f = 3$ s.

Close examination of the results given in Table 1 reveals that the proposed semi-active vibration control strategy can improve the performance of the structure significantly. For harmonic excitation, using the proposed strategy, about 15% and 45% reduction in local vibration and 20% and 38% reduction in global vibration are observed compared with the cases of 0.0 and 1.5 A constant current, respectively. Moreover, for transient excitation the results show

**Table 1 Performance index for global vibration of the whole structure and local vibration at node 19**

| Excitation | | $I = 0.0$ A | $I = 1.50$ A | $I = 0.0 - 1.50$ A |
|---|---|---|---|---|
| Harmonic | Global ($m^2 \cdot s$) | 0.0156 | 0.0201 | 0.0125 |
| | Local ($m^2 \cdot s$) | 0.0013 | 0.0020 | 0.0011 |
| Transient | Global ($m^2 \cdot s$) | 0.0052 | 0.0051 | 0.0050 |
| | Local ($m^2 \cdot s$) | 0.0028 | 0.00055 | 0.00047 |
| Random | Global ($m^2 \cdot s$) | 0.03028 | 0.02603 | 0.02319 |
| | Local ($m^2 \cdot s$) | 0.09643 | 0.08814 | 0.08316 |

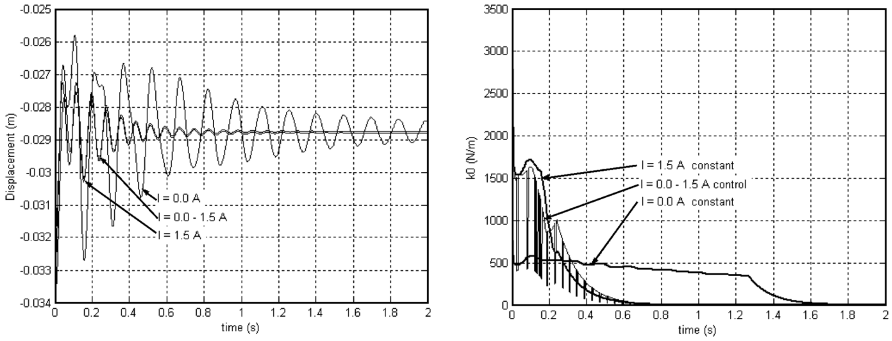


a) b)

**Fig. 12 a) Absolute *Z*-displacement of node 19 under step base excitation; b) MR damper stiffness variation under step base excitation.**

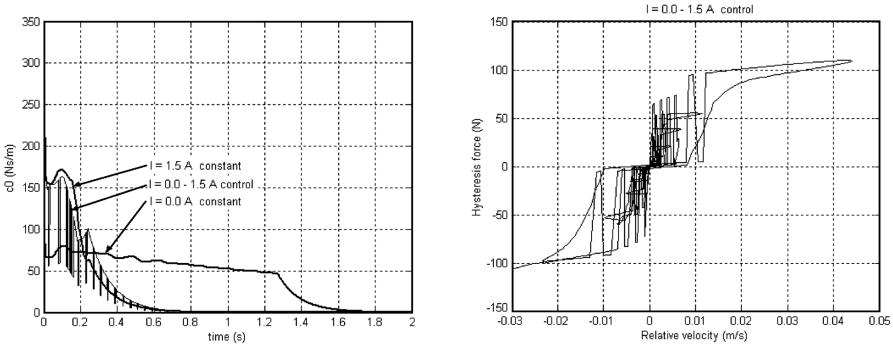


a) b)

**Fig. 13 a) MR damper damping coefficient variation under step base excitation; b) Hysteresis force in MR damper under step excitation using semi-active vibration control.**

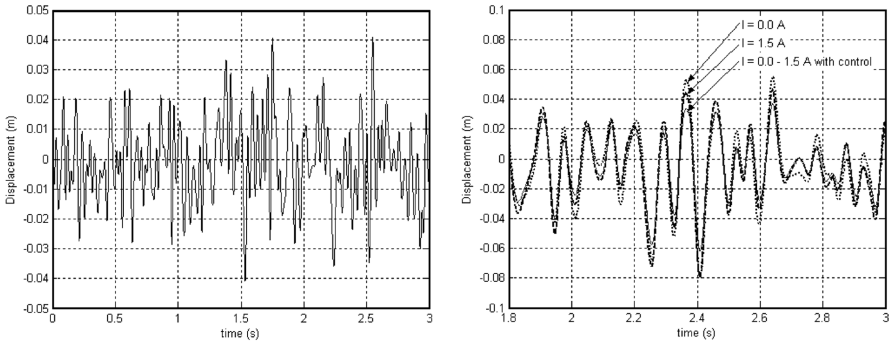


a) b)

**Fig. 14 a) Random input base excitation; b) *Z*-displacement of node 19 under random base excitation.**

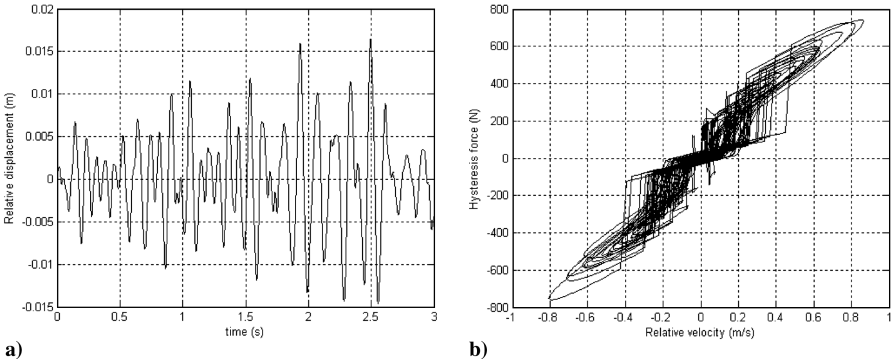


a) b)

**Fig. 15 a) Relative displacement in MR damper under random excitation using semi-active vibration control; b) Hysteresis force in MR damper under random excitation using semi-active vibration control.**

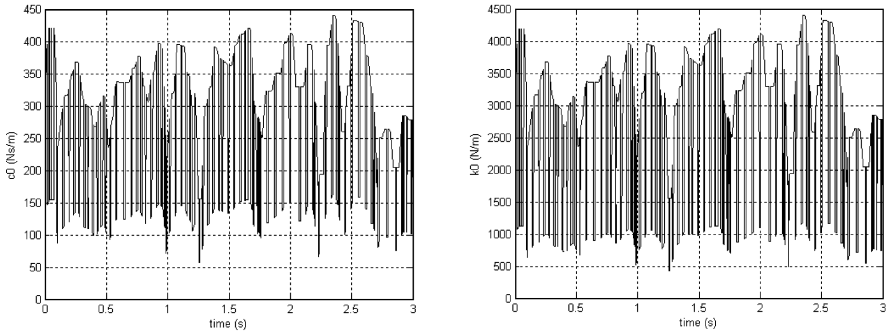


a) b)

**Fig. 16 a) MR damper damping coefficient variation under random excitation using semi-active vibration control; b) MR damper stiffness variation under random excitation using semi-active vibration control strategy.**

about 83% and 15% local vibration reduction using the proposed semi-active vibration control strategy in comparison to the cases of 0.0 and 1.5 A, respectively. For the case of random vibration, 14% and 6% local vibration reduction has been achieved using the proposed vibration control strategy compared with the cases of 0.0 and 1.5 A constant currents, respectively. The global vibration reduction using the proposed strategy for the case of random vibration excitation has been found to be 23% and 11% compared with the cases of 0.0 and 1.5 A constant current, respectively. Although a considerable reduction of global vibration of the random case has been observed, it is not as important as the harmonic and transient cases. This is mostly due to the switching transients during the ON-OFF current application. One possible way to overcome this aspect is to consider additional smoothening algorithms in switching.

## VIII. Conclusions

Semi-active vibration reduction has been achieved by integrating the MR damper in space truss structures. First the finite element model of the adaptive structure is established. To validate the finite element model, a four bays space truss structure has been fabricated and excited using a hydraulic shaker. Good agreement between the simulation and experimental results has been proved. Next, a semi-active vibration control strategy was proposed to suppress the global and local vibration of the structure using MR damper. This strategy considers the signs of the absolute velocity of one end of the MR damper in local coordinates and the hysteresis force. If the hysteresis force has the same sign of the velocity, maximum current is applied; otherwise minimum current is assumed. This semi-active vibration suppression strategy was applied and compared with the cases where the MR damper is working in passive way. It was observed that the proposed strategy significantly reduces both local and global vibration.

## Acknowledgments

Support by Natural Science and Engineering Research Council (NSERC) of Canada and Universidad Autonoma de Queretaro are gratefully acknowledged.

## References

[1] Bouc, R., "Modèle Mathématique D'hystérésis," *Acustica*, Vol. 24, No. 1, 1971, pp. 16–25.

[2] Wen, Y. K., "Method of Random Vibration of Hysteretic Systems," *Journal of Engineering Mechanics/American Society of Civil Engineers*, Vol. 102(EM2), No. 2, 1976, pp. 249–263.

[3] Spencer, B. F., Jr., Dyke, S. J., Sain, M. K., and Carlson J. D., "Phenomenological Model for Magnetorheological Dampers," *Journal of Engineering Mechanics/American Society of Civil Engineers*, Vol. 123, No. 3, 1997, pp. 230–252.

[4] Yang, G., Spencer, B. F., Jr., Jung, J. H., and Carlson, D., "Dynamic Modeling of Large-Scale Magnetorheological Damper Systems for Civil Engineering Applications," *Journal of Engineering Mechanics/American Society of Civil Engineers*, Vol. 130, No. 9, 2004, pp. 1107–1114.

[5] Choi, S. B., and Lee S. K., "A Hysteresis Model for the Field-Dependent Damping Force of a Magnetorheological Damper," *Journal of Sound and Vibration*, Vol. 245, No. 2, 2001, pp. 375–383.

[6] Wang, E. R., Ma, X. Q., Rakheja S., and Su, C. Y., "Modeling the Hysteric Characteristics of a Magnetorheological Fluid Damper," *Proceedings of the Institution of Mechanical Engineers*, Vol. 217, No. 7, Part D, 2003, pp. 537–550.

[7] Dominguez, A., Sedaghati, R., and Stiharu, I., "A New Dynamic Hysteresis Model for the Magnetorheological Dampers," *Smart Materials and Structures*, 2005 (to be published).

[8] Onoda, J., Oh, H. U., and Minesugi, K., "Semi-Active Vibration Suppression of Truss Structures by Electrorheological Fluid," *Acta Astronautica*, Vol. 40, No. 11, 1997, pp. 771–779.

[9] Dyke, D. J., Spencer, B. F., Sain, M. K., and Carlson, J. D., "Modeling and Control of Magnetorheological Dampers for Seismic Response Reduction," *Smart Materials and Structures*, Vol. 5, No. 5, 1996, pp. 565–575.

[10] Soong, T. T., and Spencer, B. F., Jr., "Supplemental Energy Dissipation: State-of-Art and State-of-the-Practice," *Engineering Structures*, Vol. 24, No. 3, 2002, pp. 243–259.

[11] Ikeda, Y., Sasaki, K., Sakamoto, M., and Kobori, T., "Active Mass Driver System as the First Application of Active Structural Control," *Earthquake Engineering and Structural Dynamics*, Vol. 30, No. 11, 2001, pp. 1575–1595.

[12] Watabe, M., Tohdo, M., Chiba, O., Izumi, N., Ebisana, H., and Fujita, T., "Response Control Performance of a Hybrid Mass Damper Applied to a Tall Building," *Earthquake Engineering and Structural Dynamics*, Vol. 30, No. 11, 2001, pp. 1655–1676.

[13] Saito, T., Shiba, K., and Tamura, K., "Vibration Control Characteristics of a Hybrid Mass Damper System Installed in Tall Buildings," *Earthquake Engineering and Structural Dynamics*, Vol. 30, No. 11, 2001, pp. 1677–1696.

[14] Ying, Z. G., Zhu, W. Q., and Soong, T. T., "A Stochastic Optimal Semi-Active Control Strategy for ER/MR Damper," *Journal of Sound and Vibration*, Vol. 259, No. 1, 2002, pp. 45–62.

[15] Zhu, W. Q., Luo, M., and Dong, L., "Semi-Active Control of Wind Excited Building Structures using ER/MR Dampers," *Probabilistic Engineering Mechanics*, Vol. 19, No. 3, 2004, pp. 279–285.

[16] Dominguez, A., Sedaghati R., and Stiharu, I., "Modeling the Hysteresis Phenomenon of Magnetorheological Dampers," *Smart Materials and Structures*, Vol. 13, No. 6, 2004, pp. 1351–1361.

[17] Rao, S. S., *The Finite Element Method in Engineering*, Butterworth–Heinemann, Woburn, MA, 1999.

[18] Wilson, E. L., *Three Dimensional Static and Dynamic Analysis of Structures, A Physical Approach with Emphasis on Earthquake Engineering*, Computers and Structures, Berkeley, CA,2002, Chaps. 19, 20.

[19] Qu, W. L., Xu, Y. L., and Lv, M. Y., "Seismic Response Control of Large-Span Machinery Building on top of Ship Lift Towers using ER/MR Moment Controllers," *Journal of Engineering Structures*, Vol. 24, No. 4, 2002, pp. 517–527.

E. Livne
*Associate Editor*